

# Description of the recently observed hypernucleus ${}^{15}_{\Xi^-}\text{C}$ within a quark-meson coupling model

R. Shyam<sup>1</sup>, K. Tsushima<sup>2</sup>

<sup>1</sup> *Theory Division, Saha Institute of Nuclear Physics,  
1/AF Bidhan Nagar, Kolkata 700064, India*

<sup>2</sup> *Laboratório de Física Teórica e Computacional,  
Universidade Cruzeiro do Sul, Rua Galvão Bueno,  
868, Liberdade 01506-000, São Paulo, SP, Brazil*

(Dated: January 21, 2019)

## Abstract

We investigate within a quark-meson coupling (QMC) model, the structure of the bound  $\Xi^-$  hypernucleus  ${}^{15}_{\Xi^-}\text{C}$  ( ${}^{14}\text{N} + \Xi^-$ ), which has been observed in a recent analysis of the KEK-E373 experiment. In the QMC model, light quarks in nonoverlapping nucleon and  $\Xi^-$  baryons interact self-consistently with isoscalar-scalar ( $\sigma$ ), isoscalar-vector ( $\omega$ ), and isovector-vector ( $\rho$ ) mesons in the mean field approximation. The parameters of the model (quark-meson coupling constants and masses) are mostly fixed from the nuclear matter saturation properties. The QMC model closely reproduces the separation energies of the two  $\Xi^-$  hyperon states in  ${}^{15}_{\Xi^-}\text{C}$  reported in the KEK-E373 analysis, and identifies their quantum numbers. We also make predictions for the cross sections for the production of the  ${}^{15}_{\Xi^-}\text{C}$  hypernuclear spectra in the  $(K^-, K^+)$  reaction on a  ${}^{15}\text{O}$  target within a covariant effective Lagrangian model using the  $\Xi^-$  bound state spinors obtained within the same QMC model.

The knowledge about the hyperon-nucleon ( $YN$ ) and hyperon-hyperon ( $YY$ ) interactions is still not of the same precision as it is for the nucleon-nucleon ( $NN$ ) interaction. This is mainly due to the fact that sufficient and precise scattering data on the  $YN$  and  $YY$  systems are not available because such experiments are difficult to perform due to the short life times of hyperons. This is of vital importance to have precise information about these interactions as they are key to the investigations of several interesting aspects in nuclear and astrophysics. This input is needed in probing the role of the strangeness in the equation of state at high density, as investigated in the cores of neutron stars [1, 2] and in high energy heavy ion collisions at relativistic heavy ion collider (RHIC) located in Brookhaven National laboratory [3], CERN [4] in Geneva and FAIR facility in GSI [5], Darmstadt.

During the last decade lattice simulations, which perform the *ab initio* calculations of quantum chromodynamics (QCD) in the nonperturbative regime, have been developed to calculate baryon-baryon interactions in both nonstrange [6–8] and strange sectors [9–13] by the HAL QCD collaboration. However, more studies are needed with improved statistics at the physical pion mass point to stabilize the results of these investigations.

The studies of hypernuclei provide another means to get useful information about the  $YN$  interaction. For the  $\Lambda$  (strangeness  $S = -1$ ) hypernuclei extensive amount of experimental data are available for some of the structure observables (like binding energies and spins) [14, 15]. This has provided important constraints (see, e.g. [16] for a recent review) on the bare  $\Lambda N$  interactions [17–23] obtained by fitting the sparsely available  $\Lambda N$  scattering data.

As far as  $\Xi$  hypernuclei are concerned, there are some hints of their existence from emulsion events [24–28]. The  $(K^-, K^+)$  reaction that leads to the transfer of two units of both charge and strangeness to the target nucleus, provides one of the most promising ways for studying the  $\Xi$  hypernuclei. However, in a few experiments performed for this reaction on a  $^{12}\text{C}$  target [29, 30], no bound state of the hypernucleus  $^{12}_{\Xi}\text{-Be}$  was unambiguously observed because of the limited statistics and detector resolution. Nevertheless, from the studies on the shapes of the continuum spectra observed in these experiments an attractive  $\Xi^-$  - nucleus potential well depth of about 14 MeV was suggested. On the other hand, in Ref. [31], a value in the range of 21–24 MeV was obtained for the depth of this potential well from the analysis of scarce emulsion data. At the same time, in a recent study [32] performed for the  $^{12}_{\Xi}\text{-Be}$  hypernucleus within a version of the QMC model [33] that is constructed for applications to the strange hyperon sector, the sum of the scalar and vector mean field potentials at the

zero radius was found to be about -21.3 MeV. This quantity, which is comparable with the depth of the conventional Woods-Saxon potential [32, 34, 35], is similar to the  $\Xi^-$ -nucleus potential depth obtained in the analysis of Ref. [31]. Thus, the  $\Xi^-$ -nucleus potential depths obtained in analyses of emulsion and spectrometer data and in alternative theoretical models differ from each other by as much as 10 MeV.

Convincing evidence for the  $\Xi$  single-particle bound states is of crucial importance for the extraction of the reliable information on the  $\Xi$  single-particle potential and the effective  $\Xi N$  interaction. Recently, in Ref. [36], the first unambiguous observation of the bound  $\Xi^-$  hypernuclear states has been reported in the  $^{14}\text{N} - \Xi^-$  system ( $^{15}_{\Xi^-}\text{C}$ ). These authors have performed new analysis of the nuclear emulsion in the E373 experiment at KEK-PS [36]. The reaction uniquely identified was  $\Xi^- + ^{14}\text{N} \rightarrow ^{15}_{\Xi^-}\text{C} \rightarrow ^{10}_{\Lambda}\text{Be} + ^5_{\Lambda}\text{He}$ . The  $\Xi^- - ^{14}\text{N}$  binding energy ( $B_{\Xi^-}$ ) was measured as  $4.43 \pm 0.25$  MeV under the assumption that both  $^{10}_{\Lambda}\text{Be}$  and  $^5_{\Lambda}\text{He}$  were produced in their ground states. However, if  $^{10}_{\Lambda}\text{Be}$  was produced in its highest excited state (with the excitation energy of 3.27 MeV), the  $B_{\Xi^-}$  was  $1.11 \pm 0.25$  MeV. This data is known as Kiso event.

In Ref. [37], the data of the Kiso event have been analyzed within the Relativistic mean field (RMF) and Skyrme-Hartree-Fock (SHF) models. The stated aim of this work was to determine theoretically if the Kiso event corresponds to  $^{14}\text{N} - \Xi^-(1s)$  or  $^{14}\text{N} - \Xi^-(1p)$  configurations, and to determine the magnitude of the attractive potential that was required to reproduce the observed binding energies of the event. However, these authors have fitted the effective interactions used in their calculations to the measured binding energy of the Kiso event, which makes their calculations some what inconsistent.

The aim of this paper is to study the Kiso event within the QMC model. In this model, light quarks within the nonoverlapping nucleon and  $\Xi^-$  bags (modeled using the MIT bag), interact self-consistently with isoscalar-scalar ( $\sigma$ ) and isoscalar-vector ( $\omega$ ) mesons in the mean-field approximation (see, e.g. [38]). The self-consistent response of the bound light quarks to the mean  $\sigma$  field leads to a new saturation mechanism for the nuclear matter [38–41]. The parameters of the QMC model (quark-meson couplings and quark masses) were fixed from the nuclear matter saturation properties (see, e.g. Table 13 of Ref. [42]). Using same set of parameters, the QMC model has been successfully applied to study the properties of finite nuclei [43] and hypernuclei [44], the binding of  $\omega$ ,  $\eta$ ,  $\eta'$  and  $D$  nuclei [45–47] and also the effect of the medium on  $J/\Psi$  production [42, 47, 48]. We emphasize that no parameter

of the model is fitted to the experimental binding of the hypernuclei under study.

We have used the QMC model [33] to predict the binding energies of the states of the  $^{15}_{\Xi}$ -C hypernucleus having the  $1s$  and  $1p$   $\Xi^-$  configurations. The corresponding scalar and vector mean fields that lead to the binding energies predicted by the model are also explicitly calculated. The upper and lower components of  $\Xi^-$  bound state spinors are calculated for each configuration, which have been employed to calculate the cross sections for the production of the  $^{15}_{\Xi}$ -C hypernuclear spectrum via the  $(K^-, K^+)$  reaction on a  $^{15}\text{O}$  target within a covariant effective Lagrangian model [32, 49]. This may be useful in identifying the states of this hypernucleus more clearly in a possible future experiment at the JPARC facility in Japan.

In the Sec. II, our formalism is briefly described, where we have given some details of the QMC model and the parameters involved therein. The results of our calculations and their discussions are given in Sec. III. The summary and conclusions of our work are described in Sec. IV.

## I. FORMALISM

In the QMC model [38, 39], quarks within the nonoverlapping nucleon and hyperon bags [44] (modeled using the MIT bag), interact self-consistently with isoscalar-scalar ( $\sigma$ ) and isoscalar-vector ( $\omega$ ) mesons in the mean field approximation. Thus, this model self-consistently relates the dynamics of the internal quark structure of a hadron to the relativistic mean fields arising in the nuclear matter.

In order to calculate the properties of finite hypernuclei, and the spinors of the bound states, we construct a simple, relativistic shell model, with the nucleon core calculated in a combination of self-consistent scalar and vector mean fields. The Lagrangian density for a hypernuclear system ( $Z$ ) in the QMC model is written as a sum of two terms,  $\mathcal{L}_{QMC}^Z =$

$\mathcal{L}_{QMC}^N + \mathcal{L}_{QMC}^{HY}$  ( $HY = \text{hyperon}$ ) [44], where,

$$\begin{aligned}
\mathcal{L}_{QMC}^N &= \bar{\psi}_N(\mathbf{r})[i\gamma \cdot \partial - M_N(\sigma) - (g_\omega \omega(\mathbf{r}) \\
&\quad + g_\rho \frac{\tau_3^N}{2} b(\mathbf{r}) + \frac{e}{2}(1 + \tau_3^N)A(\mathbf{r}))\gamma_0]\psi_N(\mathbf{r}) \\
&\quad - \frac{1}{2}[(\nabla\sigma(\mathbf{r}))^2 + m_\sigma^2\sigma(\mathbf{r})^2] \\
&\quad + \frac{1}{2}[(\nabla\omega(\mathbf{r}))^2 + m_\omega^2\omega(\mathbf{r})^2] \\
&\quad + \frac{1}{2}[(\nabla b(\mathbf{r}))^2 + m_\rho^2 b(\mathbf{r})^2] + \frac{1}{2}(\nabla A(\mathbf{r}))^2,
\end{aligned} \tag{1}$$

and

$$\begin{aligned}
\mathcal{L}_{QMC}^{HY} &= \sum_{HY=\Lambda, \Sigma, \Xi} \bar{\psi}_{HY}(\mathbf{r})[i\gamma \cdot \partial - M_{HY}(\sigma) - (g_\omega^{HY} \omega(\mathbf{r}) \\
&\quad + g_\rho^{HY} I_3^{HY} b(\mathbf{r}) + eQ_{HY}A(\mathbf{r}))\gamma_0]\psi_{HY}(\mathbf{r}).
\end{aligned} \tag{2}$$

In Eqs. (1) and (2),  $\psi_N(\mathbf{r})$ ,  $\psi_{HY}(\mathbf{r})$ ,  $\sigma(\mathbf{r})$ ,  $\omega(\mathbf{r})$  and  $b(\mathbf{r})$  are, respectively, the nucleon, hyperon,  $\sigma$ -meson,  $\omega$ -meson and  $\rho$ -meson fields, while  $m_\sigma$ ,  $m_\omega$  and  $m_\rho$  are the masses of the  $\sigma$ ,  $\omega$  and  $\rho$  mesons. The  $A(\mathbf{r})$  is Coulomb field.  $g_\omega$  and  $g_\rho$  are the  $\omega$ -N and  $\rho$ -N coupling constants, which are related to the corresponding ( $u, d$ )-quark- $\omega$  ( $g_\omega^q$ ), and ( $u, d$ )-quark- $\rho$  ( $g_\rho^q$ ) coupling constants as  $g_\omega = 3g_\omega^q$  and  $g_\rho = g_\rho^q$ . For the hyperon,  $g_\omega^{HY} = (n_0/3)g_\omega^q$  with  $n_0$  being the light-quark number in the hyperon, and  $g_\rho^{HY} \equiv g_\rho = g_\rho^q$ , where  $HY$  represents the hyperon type.  $I_3^{HY}$  and  $Q_{HY}$  are the third component of the hyperon isospin operator and its electric charge in units of the proton charge,  $e$ , respectively.

The following set of equations of motion are obtained for the hypernuclear system from the Lagrangian density Eqs. (1)-(2):

$$\begin{aligned}
&[i\gamma \cdot \partial - M_N(\sigma) - (g_\omega \omega(\mathbf{r}) + g_\rho \frac{\tau_3^N}{2} b(\mathbf{r}) \\
&\quad + \frac{e}{2}(1 + \tau_3^N)A(\mathbf{r}))\gamma_0]\psi_N(\mathbf{r}) = 0,
\end{aligned} \tag{3}$$

$$\begin{aligned}
&[i\gamma \cdot \partial - M_{HY}(\sigma) - (g_\omega^{HY} \omega(\mathbf{r}) + g_\rho^{HY} I_3^{HY} b(\mathbf{r}) \\
&\quad + eQ_{HY}A(\mathbf{r}))\gamma_0]\psi_{HY}(\mathbf{r}) = 0,
\end{aligned} \tag{4}$$

$$\begin{aligned}
&(-\nabla_r^2 + m_\sigma^2)\sigma(\mathbf{r}) = \\
&\quad g_\sigma C_N(\sigma)\rho_s(\mathbf{r}) + g_\sigma^{HY} C_{HY}(\sigma)\rho_s^{HY}(\mathbf{r}),
\end{aligned} \tag{5}$$

$$(-\nabla_r^2 + m_\omega^2)\omega(\mathbf{r}) = g_\omega \rho_B(\mathbf{r}) + g_\omega^{HY} \rho_B^{HY}(\mathbf{r}), \tag{6}$$

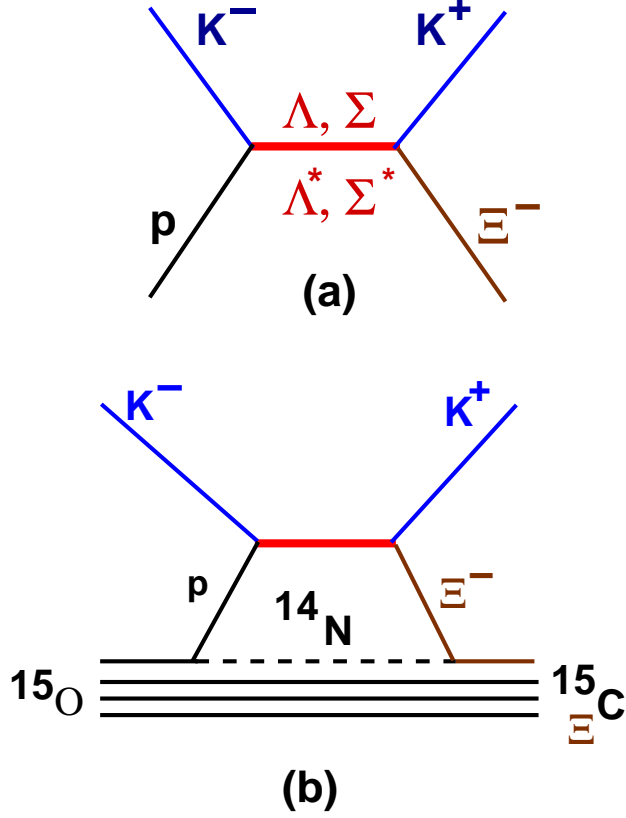


FIG. 1. (color online) Graphical representation of our model to describe  $p(K^-, K^+)\Xi^-$  (Fig. 1a) and  $^{15}\text{O}(K^-, K^+)\Xi^-^{15}\text{C}$  reactions (Fig. 1b).

$$(-\nabla_r^2 + m_\rho^2)b(\mathbf{r}) = \frac{g_\rho}{2}\rho_3(\mathbf{r}) + g_\rho^{HY} I_3^{HY} \rho_B^{HY}(\mathbf{r}), \quad (7)$$

$$(-\nabla_r^2)A(\mathbf{r}) = e\rho_p(\mathbf{r}) + eQ_{HY}\rho_B^{HY}(\mathbf{r}), \quad (8)$$

where,  $\rho_s(\mathbf{r})$  [ $\rho_s^{HY}(\mathbf{r})$ ], and  $\rho_B(\mathbf{r})$  [ $\rho_B^{HY}(\mathbf{r})$ ] are, respectively, the scalar, and baryon densities at position  $\mathbf{r}$  in the hypernucleus, while  $\rho_3(\mathbf{r})$  and  $\rho_p(\mathbf{r})$  are, respectively, the third component of isovector, and proton densities at the same position in this system [44]. On the right hand side of Eq. (5), a new and characteristic feature of QMC model appears that arises from the internal structure of the nucleon and hyperon, namely,  $g_\sigma C_N(\sigma) = -\frac{\partial M_N(\sigma)}{\partial \sigma}$  and  $g_\sigma^{HY} C_{HY}(\sigma) = -\frac{\partial M_{HY}(\sigma)}{\partial \sigma}$  where  $g_\sigma \equiv g_\sigma(\sigma = 0)$  and  $g_\sigma^{HY} \equiv g_\sigma^{HY}(\sigma = 0)$ . We use the nucleon and hyperon masses as parameterized in Ref. [33] with the corresponding parameters obtained therein. The scalar and vector fields as well as the spinors for hyperons and nucleons, can be obtained by solving these coupled equations self-consistently.

In order to provide further constraint on the ground state structure of  $^{15}_{\Xi}\text{C}$ , we have

calculated the cross sections for the production of this hypernucleus via the  $(K^-, K^+)$  reaction on a  $^{15}\text{O}$  target within an effective Lagrangian model (ELM) [32], which is similar to that used in Ref. [50] to study the elementary production reaction,  $p(K^-, K^+)\Xi^-$ . We consider only the  $s$ -channel production diagrams [see, Fig. 1(a)] as we are interested in the region where  $p_{K^-}$  lies below 2 GeV/c. The model retains the full field theoretic structure of the interaction vertices and treats baryons as Dirac particles. Figure 1(b) provides the graphical representation of the model used to describe the hypernuclear production. The initial state interaction of the incoming  $K^-$  with a bound target proton leads to excitation of intermediate  $\Lambda$  and  $\Sigma$  resonant states, which propagate and subsequently decay into a  $\Xi^-$  hyperon that gets captured into one of the nuclear orbits, while the other decay product, the  $K^+$  goes out. In Ref. [50], it was shown that six intermediate resonant states,  $\Lambda$ ,  $\Lambda(1405)$ ,  $\Lambda(1520)$ ,  $\Lambda(1810)$ ,  $\Sigma$ , and  $\Sigma(1385)$ , make the most significant contributions to the cross sections of the elementary process. Therefore, like in Ref. [32], in our present study the amplitudes corresponding to these six resonant states have been considered.

We assume the initial proton bound state to have quantum numbers of the outermost  $1p_{1/2}$  proton orbit. The pure single-hole-single-particle ( $p^{-1}\Xi^-$ ) configuration has been considered for the nuclear structure part that leads to the hypernuclear spectrum that is clearly divided into two groups:  $(1p_{1/2}^{-1}, 1s_{1/2}^{\Xi^-})$ , and  $(1p_{1/2}^{-1}, 1p_{3/2}^{\Xi^-})$ , corresponding to  $(1s_{1/2})$  and  $(1p_{3/2})$   $\Xi^-$  configurations, respectively, for the  $^{14}\text{N} - \Xi^-$  system. Since  $1p_{3/2}$  proton hole state has a much larger binding energy, any configuration mixing is expected to be negligible and has not been considered in this study.

In the calculations of the hypernuclear production cross sections with a particular ground state structure, the momentum space bound  $\Xi^-$  spinors of that state enter into the calculations. In addition, the spinors for the bound proton in the initial state are also required. These are the four component Dirac spinors, which are solutions of the Dirac equation for a bound state problem in the presence of external potential fields. They are calculated within the QMC model [33]. The use of bound state spinors determined within this model provides an opportunity to investigate the role of the quark degrees of freedom in the cascade hypernuclear production.

The proton and  $\Xi^-$  spinors are represented by  $\psi(k_p)$  and  $\psi(k_{\Xi^-})$ , respectively, later on.

We write

$$\psi(k_i) = \delta(k_{i0} - E_i) \begin{pmatrix} f(K_i)\mathcal{Y}_{\ell 1/2 j}^{m_j}(\hat{k}_i) \\ -ig(K_i)\mathcal{Y}_{\ell' 1/2 j}^{m_j}(\hat{k}_i) \end{pmatrix}. \quad (9)$$

In our notation  $k_i$  represents a four momentum, and  $\mathbf{k}_i$  a three momentum. The magnitude of  $\mathbf{k}_i$  is represented by  $K_i$ , and its directions by  $\hat{k}_i$ .  $k_{i0}$  represents the timelike component of momentum  $k_i$ . In Eq. (9),  $f(K_i)$  and  $g(K_i)$  are the radial parts of the upper and lower components of the spinor  $\psi(k_i)$  with  $i$  representing either a proton or a  $\Xi^-$ . The coupled spherical harmonics,  $\mathcal{Y}_{\ell 1/2 j}^{m_j}$ , is given by

$$\mathcal{Y}_{\ell 1/2 j}^{m_j}(\hat{k}_i) = \langle \ell m_\ell 1/2 \mu | j m_j \rangle Y_{\ell m_\ell}(\hat{k}_i) \chi_\mu, \quad (10)$$

where  $Y_{\ell m_\ell}$  represents the spherical harmonics, and  $\chi_\mu$  the spin-space wave function of a spin- $\frac{1}{2}$  particle. In Eq. (9)  $\ell' = 2j - \ell$  with  $\ell$  and  $j$  being the orbital and total angular momenta, respectively.

For the evaluation of the amplitudes corresponding to the processes shown in Fig. 1(b), one requires the effective Lagrangians at the resonance-kaon-baryon vertices and the corresponding vertex coupling constants. In addition, also needed are the propagators for spin-1/2 and spin-3/2 resonances that connect the initial and final state vertices. They have all been described in Ref. [32], and were taken to be the same in the present study. Full details of the calculations for the production cross sections of the  $\Xi^-$  hypernuclei within the ELM are given in Ref. [32] and we refer to this article for further details.

## II. RESULTS AND DISCUSSIONS

In Table I, we show the  $\Xi^-$  single-particle energies for the  $^{14}\text{N}$  nuclear core plus one  $\Xi^-$  configuration for the hypernucleus  $^{15}_{\Xi^-}\text{C}$  as predicted by the QMC model. The listed single-particle energy of a particular state can be equated with the  $\Xi^-$  removal energy (or the binding energy) of the bound  $^{14}\text{N} - \Xi^-$  system for that state.

We note from this Table that the single-particle energy of the  $^{15}_{\Xi^-}\text{C}(1s_{1/2})$  hypernuclear state predicted by the QMC model, is within less than 1 MeV of the measured value ( $4.38 \pm 0.25$  MeV) of the binding energy of the  $^{14}\text{N} - \Xi^-$  system reported in Ref. [36]. This is the case when both of the final state nuclei are produced in their ground states in the reaction  $\Xi^- + ^{14}\text{N} \rightarrow ^{15}_{\Xi^-}\text{C} \rightarrow ^{10}_{\Lambda}\text{Be} + ^5_{\Lambda}\text{He}$ , which are identified in the analysis of Ref. [36].



TABLE I.  $\Xi^-$  single-particle energies for a nuclear core ( $^{14}\text{N}$ ) plus one  $\Xi^-$  configuration of the hypernucleus  $^{15}_{\Xi^-}\text{-C}$  for different states.

State	single-particle energy (MeV)
$^{15}_{\Xi^-}\text{-C}(1s_{1/2})$	-5.366
$^{15}_{\Xi^-}\text{-C}(1p_{3/2})$	-0.779
$^{15}_{\Xi^-}\text{-C}(1p_{1/2})$	-0.099

The slight overestimate of the experimental data in the QMC calculations should be viewed in the light of the fact that we have not tried to readjust any of the parameters of the model in order to reproduce the experimental binding energies. All the parameters have been held fixed to those given in Ref. [33] and used in all the previous calculations of the  $\Xi^-$  hypernuclei [32, 34, 44] within the QMC model. Furthermore, with the same set of parameters the single-particle energy of the  $1s_{1/2}$  state of the  $^{12}_{\Xi^-}\text{-Be}$  hypernucleus is predicted to be -3.04 MeV, which is closer to the values reported in several other theoretical approaches [51, 52].

The single-particle energy of the  $^{15}_{\Xi^-}\text{-C}(1p_{3/2})$  state is -0.779 MeV, which is closer to the lower limit of the binding energy of the  $^{14}\text{N} - \Xi^-$  system ( $1.11 \pm 0.25$  MeV) if  $^{10}_{\Lambda}\text{Be}$  is produced in its highest excited state (which is supposed to be 3.27 MeV as predicted in cluster model calculations of Ref. [52]). On the other hand, the  $^{15}_{\Xi^-}\text{-C}(1p_{1/2})$  state is almost unbound. Thus as per QMC model, the state of the  $^{14}\text{N} - \Xi^-$  system observed in Ref. [36] with a binding energy of  $1.11 \pm 0.25$  MeV, is most likely to have the quantum number  $1p_{3/2}$ .

The scalar and vector mean fields calculated self-consistently within the QMC model that lead to these states are shown in Fig. 2 (a). It may be recalled that in this model the scalar and vector fields are generated by the couplings of  $\sigma$  and  $\omega$  mesons to light quarks. Because of the different masses of these mesons and their couplings to the light-quark fields the scalar and vector fields can acquire different radial dependence. We note that both the scalar and vector QMC fields have their maxima away from the point  $r = 0$  (center of the hypernucleus). In the mean field models of the finite nuclei the proton densities are somewhat pushed out as compared to those of the neutron, because of the Coulomb repulsion. In fact, the proton density distribution has a peak around 2 fm away from the

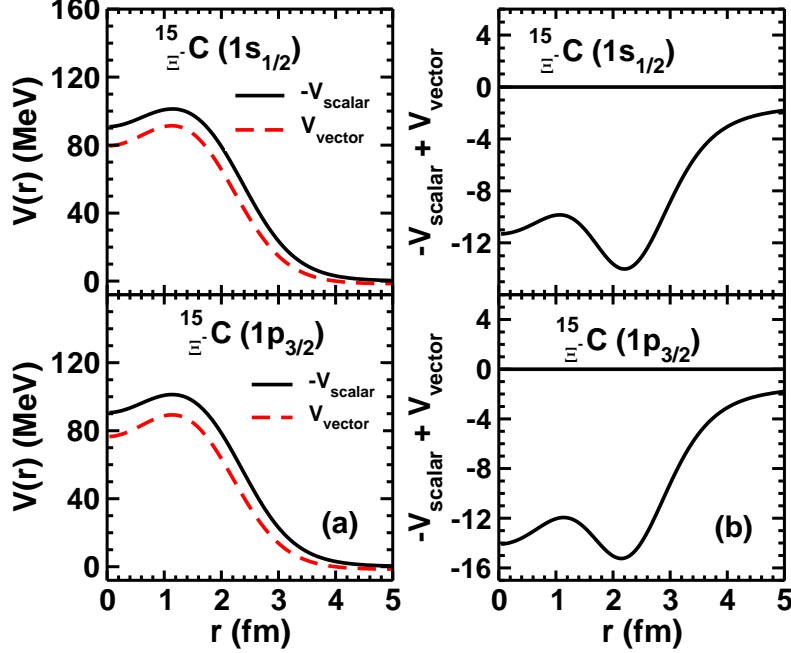


FIG. 2. (color online) (a) Vector ( $V_{vector}$ ) and scalar ( $V_{scalar}$ ) potential fields felt by  $\Xi^-$  in  $1s_{1/2}$ , and  $1p_{3/2}$  states in the hypernucleus  $^{15}_{\Xi^-}\text{C}$  as a function of the radial distance  $r$  from the center of the hypernucleus. (b) The sum  $-V_{scalar} + V_{vector}$  as a function of  $r$ .

center in  $^{15}_{\Xi^-}\text{C}$ . This causes the  $\Xi^-$  potential to have a peak around 2 fm outside of the center of the nucleus, as a consequence of the self-consistent procedure of including the Coulomb force. It may be noted that the vector potential felt by  $\Xi^-$  contains also the attractive Coulomb potential

In Fig. 2 (b), we show the quantity  $-V_{scalar} + V_{vector}$  ( $V_{NR}$ ) as a function of the radial distance  $r$  from the center of the nucleus.  $V_{NR}$  should be compared with the corresponding Woods-Saxon  $\Xi^-$  - nucleus potential of a non-relativistic theory [32, 34]. We note that at  $r = 0$ , the value of  $V_{NR}$  is about -11 MeV for the  $s$ -state and -14 MeV for the  $p$  state. This is similar to the depth of the  $\Xi^-$  -  $^{12}\text{C}$  potential assumed in Ref. [30] in order to interpret the observed spectrum of the  $(K^-, K^+)$  reaction on a  $^{12}\text{C}$  target. Interestingly,  $V_{NR}$  has a dip around  $r = 2$  fm. This is the consequence of the presence of an attractive Coulomb term in  $V_{vector}$ , due to the pushed out proton density distribution from the center of the nucleus, as already explained.

We next discuss the production of the  $^{15}_{\Xi^-}\text{C}$  hypernucleus in the  $(K^-, K^+)$  reaction on a  $^{15}\text{O}$  target. For the evaluation of the amplitudes corresponding to the processes shown in

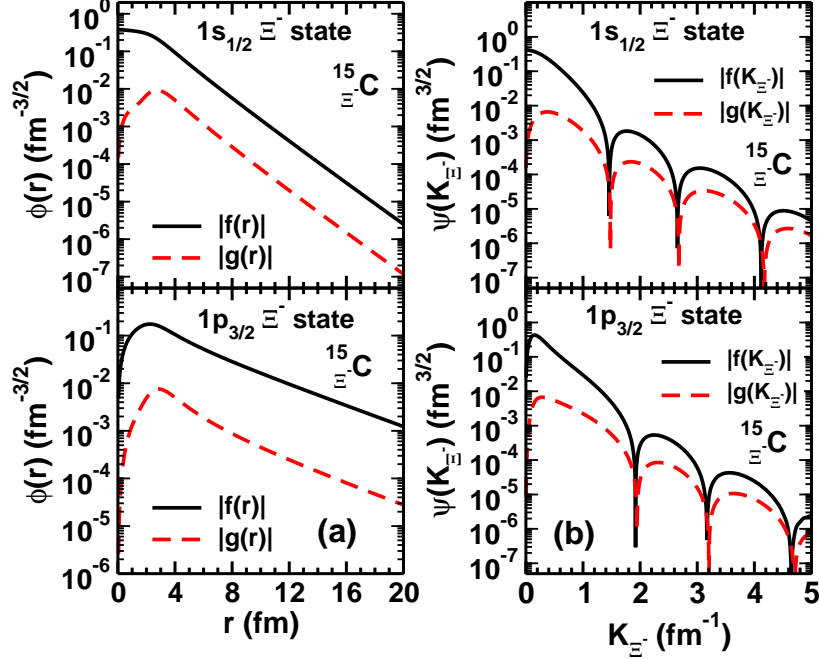


FIG. 3. (color online) (a) Moduli of the upper ( $|f(r)|$ ) and lower ( $|g(r)|$ ) components of the coordinate space spinors for  $1s_{1/2}$  and  $1p_{3/2}$   $\Xi^{-}$  states in  ${}^{15}_{\Xi^{-}}\text{C}$ . Solid lines represent the upper component while the dashed line the lower component. (b) Moduli of upper (solid lines) and lower (dashed lines) components of the momentum space spinors of the  $\Xi^{-}$  bound states in  ${}^{15}_{\Xi^{-}}\text{C}$  for the same states as in (a).

Fig. 1(b), one requires the effective Lagrangians at the resonance-kaon-baryon vertices and the corresponding vertex coupling constants. In addition, the propagators for spin-1/2 and spin-3/2 resonances that connect the initial and final state vertices, are also needed. They have all been taken from the Ref. [32]. Furthermore, the spinors for the bound proton in the initial state as well as for the bound  $\Xi^{-}$  in the final state also enter in these calculations. They have been determined within the improved QMC model [33].

Figs. 3(a) and 3(b) show the moduli of the upper and lower components of  $1s_{1/2}$ , and  $1p_{3/2}$   $\Xi^{-}$  spinors for the  ${}^{15}_{\Xi^{-}}\text{C}$  hypernucleus in coordinate space and momentum space, respectively. The spinors in the momentum space are obtained by Fourier transformation of the corresponding coordinate space spinors. We note that only for  $K$  values below  $1.5 \text{ fm}^{-1}$ , are the magnitudes of the lower components,  $|g(K)|$ , substantially smaller than those of the upper components. In the region of  $K$  pertinent to the cascade hypernuclear production,  $|g(K)|$  may not be negligible. Thus the relativistic effects resulting from the small compo-

ment of bound states spinors could be large for the hypernuclear production reactions on nuclei (see also, Ref. [53]).

In Fig. 4, we study the  $0^\circ$  differential cross sections  $[(d\sigma/d\Omega)^{0^\circ}]$  for the reaction  $K^- + {}^{15}\text{O} \rightarrow K^+ + {}^{15}_{\Xi^-}\text{C}$  obtained by using the proton-hole and  $\Xi^-$  bound state spinors calculated within the QMC model. The threshold beam momentum for this reaction is about 0.756 GeV/c, whereas that for the elementary reaction  $K^- + p \rightarrow K^+ + \Xi^-$ , is about 1.0 GeV/c. The  $\Xi^-$  hyperon in a  $1s_{1/2}$  state can populate  $0^-$  and  $1^-$  states of the hypernuclear spectrum corresponding to the hole-particle configuration  $[(p_{1p_{1/2}}^{-1}, \Xi_{1s_{1/2}}^-)]$ , while that in a  $1p_{3/2}$  state can populate  $1^+$ , and  $2^+$  states according to the configuration  $[(p_{1p_{3/2}}^{-1}, \Xi_{1p_{3/2}}^-)]$ . However, the states of unnatural parity are very weakly excited due to vanishingly small spin-flip amplitudes for this reaction [31].

In Figs. 4(a) and 4(b),  $(d\sigma/d\Omega)^{0^\circ}$  for this reaction are shown as a function of beam momentum ( $p_{K^-}$ ) for populating the hypernuclear states  $1^-$  and  $2^+$ , respectively. These are states of maximum spin with natural parity corresponding to the cases where  $\Xi^-$  hyperon is in  $1s_{1/2}$  and  $1p_{3/2}$  orbits, respectively. It is established from the studies reported in Refs. [32, 49] that within a given hole-particle configuration, states with higher angular momenta  $J$  have the larger cross sections. The configurations of the final hypernuclear states are as described in the figure captions. As stated earlier, the relative motions of  $K^-$  and  $K^+$  mesons in the initial and final channels, respectively, are described by the plane waves. However, the distortion effects are approximately accounted for by introducing a reduction factor of 3.2 to the overall cross section, which is estimated in an eikonal-approximation based procedure as discussed in Refs. [54, 55]. This method primarily takes care of the absorption effects in the incoming and outgoing channels.

In Fig. 4(a) we note that cross section rises sharply as the beam momentum increases above the reaction threshold. It peaks around  $p_{K^-} \approx 0.78$  GeV/c and falls off gradually as  $p_{K^-}$  increases further. This feature is reminiscent of the results obtained for the  ${}^{12}\text{C}(K^-, K^+){}^{12}_{\Xi^-}\text{C}$  ( $1^-$ ) reaction as shown in Ref. [32]. This is also similar to trends seen in the corresponding cross section of the elementary reaction  $p(K^-, K^+)\Xi^-$  shown in Ref. [32]. In both the cases the beam momentum distributions of the cross sections are relatively narrow.

In contrast, the beam momentum distribution of the cross sections for populating the  $2^+$  state in the  ${}^{15}\text{O}(K^-, K^+){}^{15}_{\Xi^-}\text{C}$  reaction is comparatively broad as can be seen in Fig. 4(b).

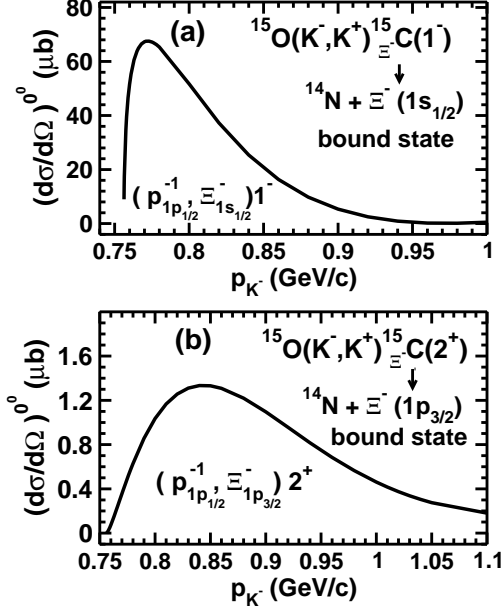


FIG. 4. (a) Calculated differential cross section at  $0^\circ$  as a function of  $K^-$  beam momentum for the  $^{15}\text{O}(K^-, K^+)_{\Xi^-}^{15}\text{C}$  reaction leading to the population of the  $1^-$  hypernuclear state within the hole-particle configuration  $(p_{1p_{1/2}}^{-1}, \Xi_{1s_{1/2}}^-)$ . These results are obtained with the QMC proton and  $\Xi^-$  bound state spinors. (b) The same as in (a) for populating the  $2^+$  hypernuclear state within hole-particle configuration  $(p_{1p_{1/2}}^{-1}, \Xi_{1p_{3/2}}^-)$ .

In this case the cross section peaks around  $p_{K^-} \approx 0.84 \text{ GeV}/c$ , which is about  $0.06 \text{ GeV}/c$  higher than that of Fig. 4(a). Also the absolute magnitudes of the cross sections are smaller in this case. This behavior has its origin in the differences in the momentum space spinors of the two states as a function of  $K_{\Xi^-}$  as shown in Fig. 3(b). The momentum transfers ( $K_{trans}$ ) involved at  $0^\circ$ , vary between  $2.30 - 3.55 \text{ fm}^{-1}$ . We note that the peaks and dips of the spinors as a function of  $K_{\Xi^-}$  of the two states do not occur at the same position. For example, at the peak positions of the cross sections in two cases (where  $K_{trans} \approx 3.00 \text{ fm}^{-1}$ ), the  $|f(K_{\Xi^-})|$  for the  $1s_{1/2}$   $\Xi^-$  state is about an order of magnitude larger than that of the  $1p_{3/2}$  state. The major reason for the different behavior of  $|f(K_{\Xi^-})|$  for the two states is the difference in the corresponding binding energies.

The different behavior of the cross sections seen in Figs. 4(a) and 4(b) could be exploited to identify the states of the  $^{15}_{\Xi^-}\text{C}$  in a possible future experiment on the  $(K^-, K^+)$  reaction on a  $^{15}\text{O}$  target.

### III. SUMMARY AND CONCLUSIONS

In this paper, we studied the structure of the hypernucleus  ${}^{15}_{\Xi^-}\text{C}$  (bound state of the  ${}^{14}\text{N} + \Xi^-$  system) within the framework of the quark-meson coupling (QMC) model. This work is motivated by the recent observation (Kiso event) that provides the first clear evidence for a strongly bound  $\Xi^-$  hypernuclear state. Recently, in Ref. [37] an analysis of this data has been performed within the relativistic mean field and Skyrme-Hartree-Fock models, where the required effective interactions were fitted to the experimental binding energy of  ${}^{15}_{\Xi^-}\text{C}$ . We do not consider this procedure to be fully consistent.

In contrast to this, none of the parameters of the QMC model (quark-meson coupling constants and quark masses) is fitted to the experimental data on the binding energy of the hypernucleus under investigation. In fact, in our present calculations the values of all the model parameters were taken to be the same as those fixed in Ref. [33] from the nuclear matter properties.

Our calculations suggest that for the Kiso event, the observed bound state of  ${}^{15}_{\Xi^-}\text{C}$  with a binding energy  $B_{\Xi^-} \approx 4.4$  MeV is the ground state of this hypernucleus having a configuration  ${}^{14}\text{N} + \Xi^-(1s_{1/2})$ . The second observed state with  $B_{\Xi^-} \approx 1.1$  MeV has a configuration  ${}^{14}\text{N} + \Xi^-(1p_{3/2})$ . This could be interpreted as an excited state of  ${}^{15}_{\Xi^-}\text{C}$  hypernucleus.

To confirm these interpretations of the Kiso event, we suggest to perform measurements on the production of  ${}^{15}_{\Xi^-}\text{C}$  hypernucleus via the  $(K^-, K^+)$  reaction on a  ${}^{15}\text{O}$  target. We have calculated the cross sections of this reaction within an effective Lagrangian model, using the proton hole and  $\Xi^-$  bound state spinors of  $s$  and  $p$  states derived from the same QMC model. We have considered the excitation of altogether six  $\Lambda$  and  $\Sigma$  hyperon resonance intermediate states in the initial collision of the  $K^-$  meson with a target proton. These states subsequently propagate and decay into a  $\Xi^-$  hyperon and a  $K^+$  meson. The hyperon gets captured in one of the nuclear orbits, while the  $K^+$  meson goes out. We find that  $\Xi^-$  hyperon in  $1s_{1/2}$  and  $1p_{3/2}$  states lead to remarkably different beam momentum distributions of the zero degree differential cross sections. This may help in distinguishing between the two states of this hypernucleus.

#### IV. ACKNOWLEDGMENTS

The work of one of the authors (RS) is supported by the Science and Engineering Research Board (SERB), Department of Science and Technology, Government of India under Grant no. SB/S2/HEP-024/2013, while the work of the other author (KT) is supported by the Conselho Nacional de Desenvolvimento Científico e Tecnológico - CNPq, Process No. 308088/2015-8, and part of the projects, Instituto Nacional de Ciência e Tecnologia - Nuclear Physics and Applications (INCT-FNA), Brazil, Process No. 464898/2014-5, and FAPESP Temático, Brazil, Process No. 2017/05660-0.

- 
- [1] J. Schaffner-Bielich, Nucl. Phys. **A 804**, 309 (2008); *ibid.* Nucl. Phys. **A 835**, 279c (2010).
  - [2] J. M. Lattimer and M. Prakash, Science **304**, 536 (2004).
  - [3] J. Adams *et al.*, Phys. Rev. Lett. **98**, 062301 (2007); J. H. Chen, Nucl. Phys. **835**, 117c (2010).
  - [4] K. Aamodt *et al.* (ALICE collaboration), Phys. Rev. Lett. **106**, 032301 (2011).
  - [5] CBM Physics Book, Springer, 2011; <http://www.gsi.de/fair/experiment/CBM/PhysicsBook.html>
  - [6] N. Ishii, S. Aoki, and T. Hatsuda, Phys. Rev. Lett. **99**, 022001 (2007).
  - [7] S. Aoki, T. Hatsuda, and N. Ishii, Progr. Theo. Phys. **123**, 89 (2010).
  - [8] N. Ishii, S. Aoki, T. Doi, T. Hatsuda, Y. Ikeda, T. Inoue, K. Murano, H. Nemura, and K. Sasaki (HAL QCD collaboration), Phys. Lett. **B712**, 437 (2012).
  - [9] H. Nemura, N. Ishii, S. Aoki and T. Hatsuda, Phys. Lett. **B673**, 136 (2009).
  - [10] T. Inoue et al. (HAL QCD collaboration), Prog. Theor. Phys. **124**, 591 (2010).
  - [11] T. Inoue, N. Ishii, S. Aoki, T. Doi, T. Hatsuda, Y. Ikeda, K. Murano, H. Nemura, and K. Sasaki et al. (HAL QCD Collaboration), Phys. Rev. Lett. **106**, 162002 (2011).
  - [12] H. Nemura, arXiv:1810.04046 [hep-lat]
  - [13] K. Sasaki, S. Aoki, T. Doi, S. Gongyo, T. Hatsuda, Y. Ikeda, T. Inoue, T. Iritani, N. Ishii, T. Miyamoto, EPJ Web of Conference **175**, 05010 (2018).
  - [14] O. Hashimoto and H. Tamura, Prog. Part. Nucl. Phys. **57**, 564 (2006).
  - [15] A. Feliciello and T. Nagae, Rep. Prog. Phys. **78**, 096301 (2015).
  - [16] A. Gal, E. V. Hungerford, and D. J. Millener, Rev. Mod. Phys. **88**, 035004 (2016).
  - [17] M. M. Nagels, T. A. Rijken and J. J. de Swart, Phys. Rev. D **20**, 1633(1979).

- [18] P. M. M. Maessen, T. A. Rijken and J. J. de Swart, Phys. Rev. C **40**, 2226 (1989).
- [19] A. Reuber, K. Holinde and J. Speth, Nucl. Phys. A **570**, 543 (1994).
- [20] T. Fujita, Y. Fujiwara, C. Nakamoto and Y. Suzuki, Prog. Theor. Phys. **100**, 931 (1998).
- [21] T. A. Rijken, V. G. J. Stoks and Y. Yamamoto, Phys. Rev. C **59**, 21 (1999).
- [22] J. Haidenbauer, Ulf-G. Meissner, Phys. Rev. C **72**, 044005 (2005).
- [23] J. Haidenbauer, Nucl. Phys. A **914**, 220c (2013).
- [24] D. H. Wilkinson *et al.*, Phys. Rev. Lett. **3**, 397 (1959)
- [25] A. Bechdolf *et al.*, Phys. Lett. **B26**, 174 (1968).
- [26] S. Aoki *et al.*, Prog. Theor. Phys. **89**, 493 (1993).
- [27] S. Aoki *et al.*, Phys. Lett. **B 355**, 45 (1995).
- [28] M. Yamaguchi, K. Tominaga, Y. Yamamoto, and T. Ueda, Prog. Theor. Phys. **105**, 627 (2001)
- [29] T. Fukuda, *et al.*, Phys. Rev. C **58**, 1306 (1998).
- [30] P. Khaustov, *et al.*, Phys. Rev. C **61**,054603(2000).
- [31] C. B. Dover and A. Gal, Ann. Phys. (NY) **146**, 309 (1983).
- [32] R. Shyam, K. Tsushima and A. W. Thomas, Nucl. Phys. **A881**, 255 (2012).
- [33] P. A. M. Guichon, A. W. Thomas, and K. Tsushima, Nucl. Phys. A **814**, 66 (2008).
- [34] R. Shyam, Nucl. Phys. A **914**, 79 (2013)
- [35] K. Tsushima, R. Shyam and A. W. Thomas, Few-Body Syst. **54**, 1271 (2013).
- [36] K. Nakazawa *et al.*, Prog. Theor. Exp. Phys. **2015**, 033D02.
- [37] T. T. Sun, E. Hiyama, H. Sagawa, H.-J. Schulze and J. Meng, Phys. Rev. C **94**, 064319 (2016).
- [38] P. A. M. Guichon, Phys. Lett. **B200**, 235 (1988).
- [39] P. A. M. Guichon, K. Saito, E. N. Rodionov, and A. W. Thomas, Nucl. Phys. **A601**, 349 (1996).
- [40] P. A. M. Guichon, H. H. Matevosyan, N. Sandulescu, A. W. Thomas, Nucl. Phys. **A772**, 1 (2006).
- [41] K. Saito and A. W. Thomas, Phys. Rev. C **51**, 2757 (1995).
- [42] K. Saito, K. Tsushima and A. W. Thomas, Prog. Part. Nucl. Phys. **58**, 1 (2007).
- [43] K. Saito, K. Tsushima and A. W. Thomas, Nucl. Phys. **A609**, 339 (1996).
- [44] K. Tsushima, K. Saito, J. Haidenbauer and A. W. Thomas, Nucl. Phys. **A630**, 691 (1998).
- [45] K. Tsushima, D. H. Lu, A. W. Thomas, and K. Saito, Phys. Lett. **B443**, 26 (1998).
- [46] K. Tsushima, D. H. Lu, A. W. Thomas, K. Saito, R. H. Landau, Phys. Rev. C **59**, 2824 (1999).



- [47] G. Krein, A. W. Thomas and K. Tsushima, Prog. Part. Nucl. Phys. **100**, 161 (2018).
- [48] A. Sibirtsev, K. Tsushima, K. Saito and A. W. Thomas, Phys. Lett. B **484**, 23 (2000).
- [49] R. Shyam, and K. Tsushima, Phys. Lett. **B 770**, 236 (2017).
- [50] R. Shyam, O. Scholten and A. W. Thomas, Phys. Rev. C **84**, 042201(R) (2011).
- [51] H. Matsumiya, K. Tsubakihara, M. Kimura, A. Dote and A. Ohnishi, Phys. Rev. C **83**, 024312 2011
- [52] E. Hiyama, Y. Yamamoto, T. Motoba, Th. A. Rijken and M. Kamimura, Phys. Rev. C **78**, 054316 (2008).
- [53] C. Bennhold and L. E. Wright, Phys. Rev. C **39**, 927 (1989); *ibid*, Phys. Lett. **B191**, 11 (1987).
- [54] R. Shyam, H. Lenske and U. Mosel, Nucl. Phys. **A 764**, 313 (2006).
- [55] R. Shyam and K. Tsushima, Phys. Rev. D **94**, 074041 (2016).